Research Square

Preprints are preliminary reports that have not undergone peer review.
They should not be considered conclusive, used to inform clinical practice,
or referenced by the media as validated information.

Discover the Active Constituents and Mechanism of Yiqi Qubai Decoction (YQD) in Treating Vitiligo based on Serum Pharmacochemistry Combining Network Pharmacology, Molecular Docking and Zebrafish Experiment

Lijun Cui
Shanghai Tongji University
Cui Ma
Shanghai Jiaotong University
Wenqing Shi
Shanghai Fourth People's Hospital Affiliated to Tongji University School of Medicine
Chen Yang
Anhui University of Chinses Medicine
Jiangping Wu
Shanghai General Hospital, Shanghai Jiaotong University School of Medicine
Zhenghua Wu
Shanghai General Hospital, Shanghai Jiaotong University School of Medicine
Yuefen lou
Shanghai Fourth People's Hospital Affiliated to Tongji University School of Medicine
Guorong Fan (fanguorong@sjtu.edu.cn)
Shanghai Tongji University

Article

Keywords: Yiqi Qubai Decoction, Vitiligo, UPLC-Q-TOF/MS, Serum pharmacochemistry, Network pharmacology, Zebrafish

Posted Date: December 7th, 2022

DOI: https://doi.org/10.21203/rs.3.rs-2327537/v1

License: This work is licensed under a Creative Commons Attribution 4.0 International License. Read Full License

Abstract

Yiqi Qubai Decoction (YQD) is composed of four herbs, namely, Astragalus propinquus Schischkin, Akebiae Fructu, Leonuri Fructus, and Caragana Sinica Roots. For decades, the decoction has been utilized in the form of granules for the treatment of vitiligo in China, with a remarkable curative result and widespread recognition among patients. However, the chemical contents and active substances of YQD absorption into the plasma, as well as its mechanism of vitiligo treatment, remain unknown. This problem was solved based on serum pharmacochemistry combining network pharmacology, molecular docking, and zebrafish experiments. First, the chemical components of YQD in vitro and the absorption components in rat plasma were identified using UPLC-Q-TOF/MS. Second, network pharmacology was integrated with molecular docking analysis to reveal the active ingredients and a putative mechanism for YQD vitiligo treatment. Finally, an in vivo zebrafish experiment validated the impact of enhancing melanin synthesis. A total of 44 chemical constituents and 36 absorption compounds, consisting of 4 prototype components and 32 metabolites were identified. Network pharmacology studies demonstrated that apigenin, astraisoflavan, akebia saponin D, genkwanin glucuronidation metabolites, and apigenin-glucuronidation metabolites might be the key active components of YQD for the treatment of vitiligo, while AKT1, mTOR, and MAPK1 may serve as the key targets. The main functional pathways involving these key targets include PI3K-AKT-mTOR, PI3K-AKT-FoxO, and MAPK signaling pathways. Molecular docking analysis found that the active components have a high affinity for AKT1, MAPK1, and mTOR. YQD could accelerate the new generation of melanin in zebrafish, which is of great significance for treating vitiligo. Our research not only looked at the absorptive and possibly useful ingredients and mechanisms of YQD for treating vitiligo, but it also confirmed the anti-vitiligo impact and served as a reference for further research, development, and application of YQD.

Introduction

Vitiligo is a common depigmentation skin condition marked by the selective death of melanocytes, resulting in the creation of white spots on the skin lesions. It is straightforward to detect but difficult to cure, with a high recurrence rate. The global incidence of vitiligo is estimated to be between 0.5% and 2%[1]. While vitiligo does not affect life expectancy, it can have a significant psychological impact and make daily life difficult. Genetic variation, autoimmune, oxidative stress, autophagy of melanocytes, neuroendocrine, and trace element insufficiency have all been linked to the pathophysiology of vitiligo[2]. These conditions can cause the death of melanocytes, resulting in the loss of pigment in the affected area. The overall role of these processes, however, is still debated. Vitiligo's etiology and pathogenesis are currently unknown. Vitiligo is currently treated with topical and systematical glucocorticoids, immunosuppressants, antioxidants, phototherapy, surgery and other methods[3-7]. However, due to side effects or expensive costs, many approaches may not achieve sufficient clinical efficacy. There is almost no cure or satisfactory treatment for certain people with a wide spectrum of lesions and a protracted course of the disease. As a result, there is a pressing need for novel medical intervention research and development.

In China, traditional Chinese medicine (TCM) has a long history of treating vitiligo, with positive results and few adverse effects. TCM syndrome differentiation of vitiligo is wind evil invasion, liver and kidney deficiency, and qi blood disharmony. During treatment, it is emphasized to soothe wind and remove dampness, soothe the liver and regulate qi, and harmonize qi blood. Professor Zhu Guangdou, a well-known Chinese dermatologist, recommended Yiqi Qubai Decoction (YQD) based on his personal experience, the principle of dialectical treatment, and clinical practice. YQD has the effect of tonifying qi, soothing the liver, activating blood, and dispelling wind, which is mainly used for the treatment of vitiligo. For decades, the decoction has been utilized in the dermatology department of Shanghai General Hospital in the form of granules, with a remarkable curative result and widespread recognition among patients. Yiqi Qubai granule has been shown to effectively diminish the patient's vitiligo disease activity (VIDA) score and has a certain effect on patients who have had the condition for more than 24 months[8]. Another study found that YQD might increase the activity of tyrosine kinase and auto-oxidize to produce melanin, resulting in anti-vitiligo effects[9]. Astragalus propinquus Schischkin (*Huang qi* in Chinese), Akebiae Fructus (*Yu zhi zi* in Chinese), Leonuri Fructus (*Chong wei zi* in Chinese), and Caragana Sinica Roots (*Jin que gen* in Chinese) (The ratio is 1:1:0.75:1.5) make up YQD. Astragalus propinquus Schischkin is a common herbal medicine with the effect of tonifying the qi of spleen and lung, immunological modulation, antioxidant, antitumor, hepatoprotective, and other functions[10-12]. It contains flavonoids, saponins, polysaccharides, and other active components. Akebiae Fructus is the dry fruit of *Akebia quinata* (Thunb.) Decne., *A. trifoliata* (Thunb.) Koidz. var. *australis* (Diels) Rehd. and *A. trifoliata* (Thunb.) Koidz. It is a well-known TCM for soothing the liver, regulating qi, activating blood circulation and relieving pain[13]. Triterpenoid saponins and triterpenoid acids are the major components of Akebiae Fructus, and they exhibit hepatoprotective, antidepressant, anticancer, anti-inflammatory, and immunomodulatory properties[14]. Leonuri Fructus is the ripe fruits of *Leonurus japonicus* (Labiatae) Houtt., which has the effect of soothing the liver and regulating qi, activating blood circulation and dispelling wind[15]. Triterpenoids, flavonoids, and sterols are the major components of Leonuri Fructus, and they have antioxidant, anti-inflammatory, and anticancer properties[16]. Caragana Sinica Roots is the root of *Caragana sinica* (Buc'hoc) Rehd., which was originally recorded in the ' Compendium of Materia Medica '. It has the effect of dispelling wind and activating blood circulation, promoting diuresis, tonifying qi and tonifying kidney[17]. The extract of Caragana Sinica Roots possesses anti-inflammatory, anti-oxidant, and anti-arthritis properties[18]. However, the active elements in YQD as well as its mode of action in the treatment of vitiligo remain unknown, and its multicomponent and multitarget properties pose significant research obstacles.

Recently, network pharmacology has been used to clarify the mechanism of disease pathogenesis and Chinese medicine's treatment of the disease, with network analysis methods being used to comprehensively analyze disease, targets, and signal pathways, which can clarify the disease mechanism, targets, and signal pathways involved in drugs[19]. The "multi-component, multi-target, and integrity" properties of TCM compound prescriptions correspond to the complex biological network of action. Therefore, network pharmacology was applied to the investigation of the mechanism of action of TCM component prescriptions[20]. A novel drug molecular screening tool was molecular docking. Computer-aided high-throughput screening of drug molecules was realized by studying the geometric and energy matching between protein macromolecular receptors and drug small molecules, and the mechanism of drug molecules was further predicted to improve its scientificity, accuracy, sensitivity, and predictability[21,22].

Previous studies have shown that the potential active ingredients of TCM were components and metabolites absorbed and/or metabolized into the blood after oral administration[23]. In this study, UPLC-Q-TOF/MS technique was used to identify the in vitro chemical components of YQD and absorbable components found in rat serum. Furthermore, serum pharmacochemistry coupled with network pharmacology and molecular docking was utilized to investigate the potential active components of YQD and the possible mechanism in treating vitiligo. Finally, zebrafish experiments were performed to confirm the pharmacological effects of YQD. To our knowledge, this is the first time to explore the serum pharmacochemistry of YQD, and it is the first report on the active ingredient of YQD and its mechanism of action in vitiligo.

Materials And Methods

Materials and Regents. Astragalus propinquus Schischkin, Akebiae Fructus, Leonuri Fructus, and Caragana Sinica Rootswere provided by Anhui Dechang Pharmaceutical Co., Ltd (Astragalus propinquus Schischkin was from Gansu Province, China. No. 20210223; Akebiae Fructus was from Henan Province, China. No. 20210314; Leonuri Fructus was from Henan Province, China. No. 20201226; Caragana Sinica Roots was from Hubei Province, China. No. 20210115). Methanol and acetonitrile (both liquid chromatography grade) were purchased from Merck (Darmstadt, Germany), and formic acid was acquired from ANPEL Lab Tech. (Shanghai, China). This assay's pure water (18.2 MΩ/cm) was deionized by a Milli-Q system (Millipore, Bedford, MA, USA). All solutions were ultrasonically degassed before use.

Preparation of YQD Sample. After soaking for 30 minutes, a total of 200 g of the four herb pieces in the prescription quantity were extracted with 8 times the amount of water for 60 minutes and promptly filtered through a 200-mesh screen. The filtrate was then extracted with 7 times the amount of water, decocted for 40 minutes, and then filtrated again. Reduced pressure condensed twice combined extraction decoction to a thick paste with a relative density of 1.35.

Animals and drug administration. Sprague-Dawley rats (180~200 g, 6~7weeks) were provided by Shanghai Silaike experimental animal Co., Ltd. (Shanghai, China, approval number: 2021-0009). Rats were kept in a separate room (24 ± 2℃, 60 ± 5% relative humidity) with the setting of a 12 h dark/light cycle. For a week before the experiment, rats were provided water and fed conventional laboratory food to acclimate. The rats were split into two groups: a control group and a YQD group (each with six rats). The rats were given 15 g/kg (dose weight/body weight) of YQD samples (dissolved in purified water) intragastrically once a day for 5 days. The rats in the control group were given the same volume of saline solution. All experiments were conducted in accordance with the Guiding Principles for the Care and Use of Laboratory Animals and were approved by the Institutional Animal Care and Use Committee (IACUC) of Shanghai Jiao Tong University (approval number A2021145). All work was performed following the recommendation of ARRIVE guidelines.

Plasma collection and preparation. At 1 h following the last dosage, blood samples were collected into an Eppendorf tube and centrifuged at 4,000 rpm for 10 min at 4°C. The plasma samples were then transferred to new tubes and kept at -80°C for analysis. To precipitate protein, 200 µl plasma was treated with 800 µl methanol, vortex mixed for 1 min, and centrifuged at 12,000 rpm for 15 min at 4°C. The supernatant was transferred to a new tube and evaporated until it was completely dry. For further analysis, the residue was redissolved in 80 µl 50% methanol and centrifuged at 12,000 rpm for 15 min.

UPLC-Q-TOF/MS analysis. Each sample was analyzed on an Agilent 1290 Infinity UPLC system (Milford, MA, USA) equipped with a Waters UPLC column (ACQUITY HSS T3, 2.1 × 100 mm, 1.8 µm). The mobile phase was as follows: solvent A (phase 0.1% formic acid aqueous solution), B (phase 0.1% formic acid acetonitrile), and linear gradient: 0~10 min, B 0; 10~27 min, B 0~15%; 27~62 min, B 15%~40%; 62~70 min, B 40%~95%; 70~75 min, B 95%; 75.01~78 min, B 0. For the analysis, a flow rate of 0.3 ml/min and a column temperature of 30°C were used. The injection volume was set at 5 µl.

The electrospray ionization source (ESI) was used by AB 4600 Q-TOF-MS/MS. The ESI source parameters were as follows: the ion spray voltage was -4.5 and 5.0 kV for the negative and positive modes, whereas the ion source temperature was 500℃. The collision energy was ±40 eV. The range of mass was m/z 50~1,250.

Target genes linked to the identified ingredients. These components discovered by UPLC-Q-TOF/MS were used to establish the chemical information database of YQD for network pharmacology study because the constituents with higher in vitro content and absorbed in the plasma were more likely bioactive chemicals. The prototype components' SMILES structure was retrieved from the Pub Chem database, and the metabolites were drawn using ChemDraw. The mol2 format was used to save all structures. Upload all structures to Swiss TargetPrediction (https://www.swiss target prediction.ch) and PharmMapper (https://www.lilab-ecust.cn/pharmmapper) prediction platforms to search for protein targets of each component, and set targets with possibility >0.1 or zscore >1.5 as potential targets with high correlation. The Uniprot database (https://www.uniprot.org) was used to transform the expected target protein names into gene names. The target proteins screened from each database were combined to remove repetitive targets.

PPI network and CTD network construction. Search and screen relevant targets in GeneCards (https://www.genecards.org), OMIM (https://www.omim.org), DisGeNET (https://www.disgenet.org), TTD (https://www.bidd.nus.edu.sg/group/cjttd), and DrugBank (https://www.drugbank.ca) databases with the keywords 'vitiligo' to obtain target gene information related to vitiligo. The target genes screened from each database were combined to remove repetitive targets.

Venn diagram of the active ingredient-disease target was created by Venny 2.1.0 software to obtain the potential target of active ingredient-disease interaction. The protein-protein interaction network (PPI) of the potential targets was drawn from String Database (https://www.string-db.org) and was analyzed by the ' Network Analysis ' function of Cytoscape 3.7.2 software. The target with a degree higher than the average value was the key target for the treatment of vitiligo.

The active ingredients and potential targets of YQD were imported into Cytoscape software to construct the compound-target-disease (CTD) network. Nodes in the network represent active ingredients, targets, and diseases, while edges represent interactions between them. For the topological properties, ‘degree’ was calculated to demonstrate the topological importance of nodes.

GO and KEGG pathway analysis. To further investigate the biological functions of vitiligo proteins, GO study was used to find this based on the Metascape database (https://metascape.org), and GO enrichment contains biological processes, molecular function, and cell localization. In addition, to confirm the pathways of these vitiligo target proteins, based on the KEGG database, a functional enrichment analysis was performed on the pathway of YQD treating vitiligo.

Molecular docking analysis. This study aimed to figure out how active chemicals interact with their protein targets and what binding mechanisms they use. As a result, we chose 11 key components and metabolites, as well as three key targets for molecular docking verification. For ingredient-target molecular docking, AutoDock Tool (ver.1.5.6) was employed.

In Vivo Zebrafish Toxicity Assay. Wild-type zebrafish embryos (AB strain) were collected from Shanghai Jiaotong University. In the toxicity assay, the embryos were incubated in a 24-well plate at 28°C from 24 hpf (post-fertilization) to 96 hpf, with 30 embryos in each well, and 2 multiple wells, with E3 medium as control and a different concentration (100, 500, 1000, 2000, and 4000 μg/ml) of YQD. Pericardium edema rate, yolk absorption delay rate, and mortality rate of zebrafish within 96 hpf after dosing were observed and recorded. GraphPad software (ver.8.0.2) was used to calculate the LC50.

In Vivo Zebrafish Pigmentation Assay. The embryos were incubated at 28°C from 24 hpf (post-fertilization) to 84 hpf in the pigmentation assay, with E3 medium as control and 100 μM 8-MOP as positive control and a variable concentration of YQD. After 84 hpf of fertilization, photographs were taken under a stereomicroscope (Olympus Instruments, Tokyo, Japan) and the melanin area of the zebrafish tail was counted with Image-Pro Plus 6.0 software.

All data have been reported as mean standard deviation. The results were analyzed and illustrated using GraphPad software. The statistical significance is described in the respective figure legends (*$P < 0.05$, **$P < 0.001$, One-way ANOVA).

Results

Identification of chemical constituents in YQD by UPLC-Q-TOF/MS. To study the absorbable components of YQD, it is necessary to analyze and identify its complex chemical components in vitro. UPLC-Q-TOF/MS was used for qualitative analysis of YQD. The MS data were first matched with the Natural Products HR-MS/MS Spectral Library 1.0 database for identification. The database contains multistage mass spectrograms of more than 1000 Chinese herbal reference substances, including different collection modes, different admixture ions, different collision energies, etc., with comprehensive information of compounds, and all of them are standard chromatograms of the actual collection, with high accuracy of matching results. The compounds not included in the database were identified according to literature reports and the pyrolysis law of mass spectrometry.

According to the multistage mass spectrometry information of the samples, combined with the high-resolution mass spectrometry database of natural products and related literature, 44 compounds were finally identified from YQD samples, including 20 triterpenoids and their glycosides, 10 flavonoids and their glycosides, 4 glycosides, 3 alkaloids, 1 stilbene and 6 organic acids (as shown in Fig. 1 and Table 1).

ID	RT (min)	adduction	*m/z*	ppm	Formula	MW	Name	MS/MS(*m/z*)
C1	0.99	$[M+H]^+$	118.0854	-7.2	$C_5H_{11}NO_2$	117.08	Betaine	118.0849;58.0636
C2	1.23	$[M+H]^+$	144.1011	-5.6	$C_7H_{13}NO_2$	143.09	Stachydrine	144.1004;84.0798;58.0642
C3	18.55	$[M-H]^-$	431.1208	3.0	$C_{18}H_{24}O_{12}$	432.13	Asperulosidic acid	431.1207;137.0244;93.0354
C4	18.96	$[M-H]^-$	313.0945	5.1	$C_{14}H_{18}O_8$	314.10	Glucovanillin	151.0404;123.0453
C5	19.49	$[M-H]^-$	353.0890	3.4	$C_{16}H_{18}O_9$	354.10	Neochlorogenic acid	353.0900;191.0574;179.0356;135.0459
C6	20.56	$[M-H]^-$	593.2094	1.2	$C_{25}H_{38}O_{16}$	594.22	Leonuriside B	593.2054;461.1655;135.0437
C7	23.06	$[M-H]^-$	353.0884	1.7	$C_{16}H_{18}O_9$	354.10	Chlorogenic acid	191.0562;85.0292
C8	23.82	$[M-H]^-$	353.0908	8.5	$C_{16}H_{18}O_9$	354.10	Cryptochlorogenic acid	353.0915;191.0577;179.0364;173.0469;135.046
C9	25.60	$[M-H]^-$	463.1274	6.1	$C_{22}H_{24}O_{11}$	464.13	Hesperetin 7-O-glucoside	463.1230;301.0662;273.0735
C10	28.62	$[M+H]^+$	312.1540	-4.5	$C_{14}H_{21}N_3O_5$	311.14	Leonurine	312.1588;181.0482;114.0997
C11	30.41	$[M-H]^-$	301.0742	8.1	$C_{16}H_{14}O_6$	302.08	Carasinaurone	301.0692;257.0832;139.0398;124.0155
C12	30.86	$[M+H]^+$	447.1269	-4.9	$C_{22}H_{22}O_{10}$	446.12	Calycosin-7-O-β-D-glucoside	285.0750;270.0517;253.0507;242.0541;225.052 137.0217
C13	33.14	$[M-H]^-$	477.1419	3.5	$C_{23}H_{26}O_{11}$	478.15	Calceolarioside B	477.1409;315.1073;161.0253;133.0296
C14	34.08	$[M-H]^-$	515.1211	3.1	$C_{25}H_{24}O_{12}$	516.13	Isochlorogenic acid B	515.1205;353.0871;191.0561;173.0452;135.045
C15	34.81	$[M-H]^-$	515.1212	3.3	$C_{25}H_{24}O_{12}$	516.13	Isochlorogenic acid A	515.1207;353.0871;191.0565;179.0363;135.045
C16	35.70	$[M-H]^-$	461.1461	1.7	$C_{23}H_{26}O_{10}$	462.15	Methylnissolin-3-O-glucoside	461.1452;179.0371;161.0245;133.0303
C17	36.68	$[M-H]^-$	515.1202	1.4	$C_{25}H_{24}O_{12}$	516.13	Isochlorogenic acid C	515.1195;353.0877;191.0558;173.0460;135.045
C18	38.03	$[M+FA-H]^-$	475.1247	0.2	$C_{22}H_{22}O_9$	430.13	Ononin	267.0691;252.0458
C19	39.14	$[M+H]^+$	1075.5261	-5.5	$C_{52}H_{82}O_{23}$	1074.52	Mutongsaponin B	943.4894;797.4332;635.3815;
C20	40.41	$[M+FA-H]^-$	987.4837	3.1	$C_{47}H_{74}O_{19}$	942.48	Saponin Ph	987.4972;941.4768;469.1586
C21	42.03	$[M-H]^-$	283.0617	1.8	$C_{16}H_{12}O_5$	284.07	Genkwanin	283.0595;268.0382;211.0388;195.0456
C22	42.08	$[M-H]^-$	463.1636	5.7	$C_{23}H_{28}O_{10}$	464.17	Astraisoflavan-7-O-β-D-glucoside	463.1615;301.1061;179.0690
C23	42.61	$[M+FA-H]^-$	1003.5116	-0.3	$C_{48}H_{78}O_{19}$	958.51	Scheffoleoside A	1003.5117;957.4984;487.3411;469.1534
C24	42.79	$[M+H]^+$	1091.5630	-0.2	$C_{53}H_{86}O_{23}$	1090.56	Akebia saponin PJ1	959.5186;813.4651;651.4084;489.3562
C25	43.64	$[M-H]^-$	431.1011	6.3	$C_{21}H_{20}O_{10}$	432.11	Apigenin 7-O-glucoside	431.0989;269.0444
C26	43.96	$[M+FA-H]^-$	1003.5218	9.8	$C_{48}H_{78}O_{19}$	958.51	Asiaticoside	1003.5229;957.5041;487.3487;469.1570
C27	44.10	$[M+H]^+$	1091.5579	-4.9	$C_{53}H_{86}O_{23}$	1090.56	23-Hydroxyakemisaponin A	959.5174;813.4715;651.3946;489.3537
C28	44.73	$[M+FA-H]^-$	1003.5154	3.5	$C_{48}H_{78}O_{19}$	958.51	(2α,3β,6β)-2,3,6-trihydroxy-Olean-12-en-28-oic acid-O-6-deoxy-α-L-mannopyranosyl-(1→4)-O-β-D-glucopyranosyl-(1→6)-β-D-glucopyranosyl ester	1003.5123;957.5028;487.3442;469.1551
C29	45.53	$[M+FA-H]^-$	969.2802	-2.1	$C_{56}H_{44}O_{13}$	924.28	Kobophenol A	923.2608;801.2261
C30	49.65	$[M+FA-H]^-$	1105.5449	1.2	$C_{52}H_{84}O_{22}$	1060.54	Akebia saponin E	1105.5482;1059.5363;735.4314
C31	50.52	$[M+FA-H]^-$	973.5077	6.5	$C_{47}H_{76}O_{18}$	928.50	Akebia saponin D	973.5041;927.4953;603.3886;323.0972;179.056
C32	51.88	$[M-H]^-$	267.0656	-2.6	$C_{16}H_{12}O_4$	268.07	Formononetin	267.0668;252.0436;195.0444;135.0122
C33	55.19	$[M+Cl]^-$	933.4640	2.1	$C_{46}H_{74}O_{17}$	898.49	(3β,4α)- 3-[(O-α-L-	933.4631;735.4207

							arabinopyranosyl-(1→2)-O-[β-D-glucopyranosyl-(1→4)]-α-L-arabinopyranosyl)oxy]-23-hydroxy-Olean-12-en-28-oic acid	
C34	56.36	$[M+FA-H]^-$	1089.5523	3.3	$C_{52}H_{84}O_{21}$	1044.55	Yuzhizioside IV	1089.5504;1043.5381;719.4348;323.0966
C35	59.25	$[M+FA-H]^-$	871.4718	2.4	$C_{43}H_{70}O_{15}$	826.47	Astragaloside	871.4730;825.4697;765.4370
C36	61.63	$[M+FA-H]^-$	871.4689	-0.9	$C_{43}H_{70}O_{15}$	826.47	Astrasieversianin VII	871.4678;825.4468
C37	63.61	$[M+FA-H]^-$	871.4731	3.9	$C_{43}H_{70}O_{15}$	826.47	Cyclosiversioside D	871.4665;825.4716;765.4327
C38	63.95	$[M+FA-H]^-$	957.5079	-4.6	$C_{47}H_{76}O_{17}$	912.51	Pulsatilla Saponin D	911.4976;749.4245
C39	64.27	$[M-H]^-$	487.3428	-0.2	$C_{30}H_{48}O_5$	488.35	Arjunolic acid	487.3422;363.0096;322.9947
C40	64.84	$[M+FA-H]^-$	781.4380	0.0	$C_{40}H_{64}O_{12}$	736.44	Akebia saponin B	781.4406;735.4318;603.3912
C41	65.12	$[M+FA-H]^-$	913.4847	4.9	$C_{45}H_{72}O_{16}$	868.48	Astragaloside	913.4814;867.4702;765.4267
C42	65.59	$[M-H]^-$	269.0474	6.9	$C_{15}H_{10}O_5$	270.05	Apigenin	269.0484;225.0556
C43	65.71	$[M+FA-H]^-$	913.4814	1.3	$C_{45}H_{72}O_{16}$	868.48	Isoastragaloside	913.4861;867.4913
C44	66.41	$[M+FA-H]^-$	913.4859	6.2	$C_{45}H_{72}O_{16}$	868.48	Neoastragaloside I	/

Table 1. Characterization of chemical components of YQD by UPLC-Q-TOF/MS.

Identification of YQD absorption ingredients and metabolites in rat plasma. After intragastric administration of YQD for 5 days, the rat plasma was collected at 1 h after the last dosing. Due to the complex chemical composition of YQD and the interaction with the body after intragastric administration, the exposure of the original chemical composition in vitro may be different and metabolites may be generated, which increases the complexity of the sample. We used UPLC-Q-TOF/MS technology to identify 36 components in rat serum, including 4 prototype components and 32 metabolites, through background reduction (blank plasma), baseline calibration and molecular characteristic extraction. The UPLC-TOF/MS graph was shown in Fig. 2. The prototype components were stachydrine (P1), carasinaurone (P2), calycosin-7-O-β-D-glucoside (P3), and akebia saponin B (P4). Among them, stachydrine and calycosin-7-O-β-D-glucoside were included in the content determination of Astragalus propinquus Schischkin and Leonuri Fructus in "Chinese Pharmacopoeia" (2022 English version) as the quality control indexes of these two herbs[24]. Carasinaurone and akebia saponin B were pharmacologically active signature ingredients from Caragana Sinica Roots and Akebiae Fructus[25]. The metabolites included hydroxylation, glucuronidation, sulfation, and compound reaction products of compounds such as calycosin-7-O-β-D-glucoside, apigenin, calycosin, genkwanin, and formononetin. The components of C13, C24, C30, and C31 with high in vitro response did not find prototype drugs or metabolites in vivo due to the low oral bioavailability and short half-life[26-28].

The quasi-molecular ion peak $[M-H]^-$ *m/z* of metabolites M2 and M16 were 621.1509 ($C_{28}H_{30}O_{16}$) and 459.0965 ($C_{22}H_{20}O_{11}$), respectively, which were 176 ($C_6H_6O_6$) higher than those of calycosin-7-O-β-D-glucoside and calycosin, and the secondary fragment ions of M2 were 283.0598; 268.0344 were similar to calycosin-7-O-β-D-glucoside, M16 secondary fragment ion 268.0383;175.0251 were similar to calycosin, so it was speculated that M2 was glucuronidation of calycosin-7-O-β-D-glucoside and M16 was glucuronidation of calycosin. Similarly, metabolites M10, M23, M6, and M27 were speculated to be glucuronide products of apigenin, formononetin, genkwanin, and methylnissolin, respectively.

The quasi-molecular ion peak $[M-H]^-$ *m/z* of metabolite M5 is 525.0383 ($C_{21}H_{18}O_{14}S$), 176 ($C_6H_6O_6$), and 80 (SO_3) higher than apigenin, with the secondary fragment ion *m/z* 269.0465, so it was speculated to be the sulfated and glucuronidated product of apigenin. The $[M-H]^-$ *m/z* of M9 was 541.0343, which was 176 ($C_6H_6O_6$), 80 (SO_3), and 17 (-OH) higher than that of apigenin. It was speculated that M9 was the hydroxylation, sulfation, and glucuronidation of apigenin. All identified results were listed in Table 2 and Table 3. The possible metabolic pathways of 32 metabolites in rats after intragastric administration of YQD were shown in Fig. 3.

ID	RT(min)	adduct ion	Protonated *m/z*	ppm	Formula	Name	MS/MS(*m/z*)
P1(C2)	1.4	$[M+H]^+$	144.1015	-2.8	$C_7H_{13}NO_2$	Stachydrine	144.1019;84.0803;58.0649
P2(C11)	30.8	$[M-H]^-$	301.0727	3.1	$C_{16}H_{14}O_6$	Carasinaurone	273.0734;241.0522;193.09778;139.0410;124.0178
P3(C12)	31.58	$[M-H]^-$	447.1281	-1.1	$C_{22}H_{22}O_{10}$	Calycosin-7-O-β-D-glucoside	447.1179;285.0760;270.0554;253.0519
P4C40)	65.48	$[M+FA-H]^-$	781.443	6.4	$C_{40}H_{64}O_{12}$	Akebia saponin B	781.4385;735.4349;603.4002;471.3462

Table2. Identification of absorbed prototype components in rat plasma by UPLC-Q-TOF/MS (1 h after the last administration).

ID	RT(min	adduct ion	Protonated *m/z*	ppm	Formula	Name	MS/MS(*m/z*)
M1	25.83	$[M-H]^-$	509.0444	9.6	$C_{21}H_{18}O_{13}S$	Daidzein+sulfation+glucuronidation	509.0428;333.0092;253.0533
M2	27.92	$[M-H]^-$	621.1509	7.7	$C_{28}H_{30}O_{16}$	Calycosin-7-O-β-D-glucoside+glucuronidation	621.1492;459.0957;283.0598;268.
M3	28.14	$[M-H]^-$	509.0421	5	$C_{21}H_{18}O_{13}S$	Daidzein+sulfation+glucuronidation	509.0419;429.0845;333.0045;253.
M4	28.74	$[M-H]^-$	429.0852	5.8	$C_{21}H_{18}O_{10}$	Daidzein+glucuronidation	253.0516;175.0232
M5	28.89	$[M-H]^-$	525.0383	7.3	$C_{21}H_{18}O_{14}S$	Apigenin+sulfation+glucuronidation	525.037;349.0028;269.0465
M6	29.71	$[M-H]^-$	459.0946	2.9	$C_{22}H_{20}O_{11}$	Genkwanin+glucuronidation	459.0964;283.0616;268.0389;240.
M7	30.73	$[M-H]^-$	497.0803	8.8	$C_{21}H_{22}O_{12}S$	Equol+sulfation+glucuronidation	497.0783;417.1204;321.0443;241.
M8	31.56	$[M-H]^-$	429.0843	3.7	$C_{21}H_{18}O_{10}$	Daidzein+glucuronidation	429.0854;253.0514;129.0216;113.
M9	31.69	$[M-H]^-$	541.0343	9.1	$C_{21}H_{18}O_{15}S$	Apigenin+hydroxylation+glucuronidation+sulfation	541.0362;461.0689;285.0416
M10	33.11	$[M-H]^-$	445.0804	6.2	$C_{21}H_{18}O_{11}$	Apigenin+glucuronidation	445.0784;269.0466;224.0483;175.
M11	33.71	$[M-H]^-$	433.1162	5	$C_{21}H_{22}O_{10}$	2',4',7-trihydroxyisoflavan+glucuronidation	433.1113;296.9257;257.0834;175.
M12	33.76	$[M-H]^-$	491.1604	9.2	$C_{24}H_{28}O_{11}$	7-hydroxy-2',3',4'-trimethoxyisoflavan+glucuronidation	491.1598;315.1253;271.1348
M13	34.69	$[M-H]^-$	445.0804	6.2	$C_{21}H_{18}O_{11}$	Apigenin+glucuronidation	445.2026;269.0479;180.0724
M14	34.7	$[M-H]^-$	333.0099	7.4	$C_{15}H_{10}O_7S$	Daidzein+sulfation	333.0087;253.0519;224.0475;117.
M15	35.07	$[M-H]^-$	447.0971	8.5	$C_{21}H_{20}O_{11}$	7,3',4'-trihydroxyisoflavanone+glucuronidation	447.0978;271.0639;198.9095;165.
M16	35.51	$[M-H]^-$	459.0965	7	$C_{22}H_{20}O_{11}$	Calycosin+glucuronidation	459.0955;283.0612;268.0383;175.
M17	35.57	$[M-H]^-$	417.1225	8.1	$C_{21}H_{22}O_9$	Equol+glucuronidation	417.1227;399.1180;241.0886;175.
M18	35.91	$[M-H]^-$	447.0943	2.3	$C_{21}H_{20}O_{11}$	7,3',4'-trihydroxyisoflavanone+glucuronidation	447.1322;271.0639;151.0070;113.
M19	36.08	$[M-H]^-$	417.1213	5.3	$C_{21}H_{22}O_9$	Equol+glucuronidation	417.1217;399.1248;241.0871;175.
M20	36.19	$[M-H]^-$	639.1964	5.2	$C_{29}H_{36}O_{16}$	Astraisoflavan-7-O-β-D-glucoside+glucuronidation	639.1995;463.1635;301.1093;286.
M21	38.65	$[M-H]^-$	417.1222	7.4	$C_{21}H_{22}O_9$	Equol+glucuronidation	417.1185;241.0917;175.0278;121.
M22	38.73	$[M-H]^-$	321.0458	6.1	$C_{15}H_{14}O_6S$	Equol+sulfation	321.0475;241.0886;121.0303
M23	38.92	$[M-H]^-$	443.0999	3.5	$C_{22}H_{20}O_{10}$	Formononetin+glucuronidation	443.1701;267.0670;252.0441;223.
M24	39.99	$[M-H]^-$	253.0526	7.8	$C_{15}H_{10}O_4$	Formononetin+demethylation	253.0518;225.0558;135.0094
M25	40.86	$[M-H]^-$	433.1153	3	$C_{21}H_{22}O_{10}$	2',4',7-trihydroxyisoflavan+glucuronidation	433.2095;257.0832;175.0253;113.
M26	41.42	$[M-H]^-$	433.1157	3.9	$C_{21}H_{22}O_{10}$	2',4',7-trihydroxyisoflavan+glucuronidation	433.1166;257.0826;136.0182
M27	41.79	$[M-H]^-$	475.1275	9.5	$C_{23}H_{24}O_{11}$	Methylnissolin+glucuronidation	475.1302;299.0936;284.0711;269.
M28	42.85	$[M-H]^-$	459.0967	7.4	$C_{22}H_{20}O_{11}$	Calycosin+glucuronidation	459.0937;283.0615;268.0368;254.
M29	43.06	$[M-H]^-$	477.1442	8.3	$C_{23}H_{26}O_{11}$	Astraisoflavan+glucuronidation	477.1445;301.1094;286.0867;271.
M30	43.28	$[M+H]^+$	303.1212	-4.9	$C_{17}H_{18}O_5$	Astraisoflavan	303.1024;167.0699;133.0677;123.
M31	44.51	$[M-H]^-$	445.1154	3.1	$C_{22}H_{22}O_{10}$	Formononetin+hydrogenation+glucuronidation	445.1165;269.0850;254.0608;217.
M32	45.67	$[M-H]^-$	347.0249	5.2	$C_{16}H_{12}O_7S$	Formononetin+sulfation	347.0290;267.0691;252.0453;223.

Table 3. Identification of metabolites in rat plasma by UPLC-Q-TOF/MS (1 h after the last administration).

Bioactive ingredients and potential targets of YQD. From the aforesaid, four absorbed components and 22 metabolites compounds were chosen for further network pharmacology studies. Daidzein and equol metabolites came from a variety of places and cannot be employed as distinct YQD metabolites[29], thus they were deleted. In addition, four components with high response values in the in vitro chemical composition spectrum, as well as apigenin, the prototype component that creates more metabolites, were added for network pharmacological prediction. Above 31 ingredient compounds used for network pharmacology analysis were shown in Table 4. In total, 466 targets related to the 31 compounds in YQD were discovered. (Supplement Table S1).

ID	Name	Formula	MW
C13	Calceolarioside B	$C_{23}H_{26}O_{11}$	478.15
C24	Akebia saponin PJ1	$C_{53}H_{86}O_{23}$	1090.56
C30	Akebia saponin E	$C_{52}H_{84}O_{22}$	1060.54
C31	Akebia saponin D	$C_{47}H_{76}O_{18}$	928.50
C42	Apigenin	$C_{15}H_{10}O_5$	270.05
P1	Stachydrine	$C_7H_{13}NO_2$	143.09
P2	Carasinaurone	$C_{16}H_{14}O_6$	302.08
P3	Calycosin-7-O-β-D-glucoside	$C_{22}H_{22}O_{10}$	446.12
P4	Akebia saponin B	$C_{40}H_{64}O_{12}$	736.44
M2	Calycosin-7-O-β-D-glucoside+glucuronidation	$C_{28}H_{30}O_{16}$	622.15
M5	Apigenin+sulfation+glucuronidation	$C_{21}H_{18}O_{14}S$	526.04
M6	Genkwanin+glucuronidation	$C_{22}H_{20}O_{11}$	460.10
M9	Apigenin+hydroxylation+glucuronidation+sulfation	$C_{21}H_{18}O_{15}S$	542.04
M10	Apigenin+glucuronidation	$C_{21}H_{18}O_{11}$	446.08
M11	4,7,4'-trihydroxyisoflavan+glucuronidation	$C_{21}H_{22}O_{10}$	434.12
M12	7-hydroxy-2',3',4'-trimethoxyisoflavan+glucuronidation	$C_{24}H_{28}O_{11}$	492.16
M13	Apigenin+glucuronidation	$C_{21}H_{18}O_{11}$	446.08
M15	7,3',4'-trihydroxyisoflavanone+glucuronidation	$C_{21}H_{20}O_{11}$	448.10
M16	Calycosin+glucuronidation	$C_{22}H_{20}O_{11}$	460.10
M18	7,3',4'-trihydroxyisoflavanone+glucuronidation	$C_{21}H_{20}O_{11}$	448.10
M20	Astraisoflavan-7-O-β-D-glucoside+glucuronidation	$C_{29}H_{36}O_{16}$	640.20
M23	Formononetin+glucuronidation	$C_{22}H_{20}O_{10}$	444.11
M24	Formononetin+demethylation	$C_{15}H_{10}O_4$	254.06
M25	4,7,4'-trihydroxyisoflavan+glucuronidation	$C_{21}H_{22}O_{10}$	434.12
M26	4,7,4'-trihydroxyisoflavan+glucuronidation	$C_{21}H_{22}O_{10}$	434.12
M27	Methylnissolin+glucuronidation	$C_{23}H_{24}O_{11}$	476.13
M28	Calycosin+glucuronidation	$C_{22}H_{20}O_{11}$	460.10
M29	Astraisoflavan+glucuronidation	$C_{23}H_{26}O_{11}$	478.15
M30	Astraisoflavan	$C_{17}H_{18}O_5$	302.12
M31	Formononetin+hydrogenation+glucuronidation	$C_{22}H_{22}O_{10}$	446.12
M32	Formononetin+sulfation	$C_{16}H_{12}O_7S$	348.03

Table 4. Information Table on Active Components of YQD

PPI and CTD Network Analysis. The target genes related to vitiligo were searched in the GeneCards, OMIM, DisGeNET, TTD, and DrugBank, Using VENNY 2.1 software to create the YQD-vitiligo overlapping targets Venn diagram, 78 overlapping targets were identified by matching the 1059 genes with the vitiligo-associated genes (Fig. 4A, Supplement Table S2). Based on the above 78 targets, the PPI network was successfully constructed and visualized (Fig. 4B, Supplement Table S3). In this PPI network, the average values of degree, betweenness, and closeness were 14.00, 0.014, and 0.515, respectively. Figure 4C depicted the top 20 targets with the highest degree, 13 of which had the above three characteristics higher than the average value, and these targets were chosen as the core targets, including AKT1, TNF, mTOR, and MAPK1 (Table 5).

Gene	Degree	Betweenness	Closeness
AKT1	52	0.165	0.772
TNF	48	0.110	0.732
ALB	46	0.113	0.732
MTOR	34	0.036	0.634
ESR1	33	0.066	0.645
CASP3	33	0.049	0.645
IGF1	32	0.026	0.628
PPARG	32	0.055	0.617
PTGS2	32	0.051	0.634
IL2	30	0.027	0.602
MAPK1	24	0.037	0.582
PIK3CA	23	0.020	0.568
SOD2	19	0.019	0.573

Table5. PPI core targets and related parameters

To elucidate the underlying relationship between the active components of YQD and key targets in the treatment of vitiligo, we constructed a compound-target-disease (CTD) network, as shown in Figure 4D. There were 111 nodes in the network, with 31 ingredients, 78 target genes, 1 illness (vitiligo), and 1 drug (YQD) among them, as well as 599 compound-target interactions. Among them, M30, M24, C42, M32, M10, M13, M15, M6, P3, and C31 ranked the top 10 in the degree of components, and these molecules may regulate multiple targets to perform therapeutic roles. The key nodes and their degree values were listed in Supplement Table S4.

GO and KEGG enrichment analysis. According to GO classification enrichment analysis, vitiligo targets were categorized as stress response, activation of cytokines, biological regulation, and cell communication (Fig. 5A). In the biological processes' analysis, these targets were enriched in the response to xenobiotic stimuli, response to the hormone, and regulation of defense response. In the cellular component's class, vitiligo targets were involved in the cytoplasmic side of the membrane, the perinuclear region of the cytoplasm, and the transcription regulator complex. In the molecular functions' category, vitiligo targets were involved in nuclear receptor activity, oxidoreductase activity, and phosphotransferase activity.

The KEGG enrichment study was carried out using the Metascape platform, and 160 pathways were discovered as a result. The top 20 important pathways related to the therapy of vitiligo, according to the FDR value of KEGG analysis, include pathways in cancer, lipid and atherosclerosis, proteoglycans in cancer, and chemical carcinogenesis-reactive oxygen species (Fig. 5B and Supplement Table S5). TNF signaling pathway, FoxO signaling pathway, PI3K-Akt signaling pathway, mTOR signaling pathway, and other signal transduction pathways were also included.

We created the component-target-pathway (CTP) network by combining the target and pathway information from the top 20 KEGG pathways with the active components to further investigate the link between active ingredients, putative targets, and pathways (Fig. 5C). The network shows 92 nodes, including 31 components, 20 pathways, and 41 targets. M30, C42, M10, M15, M24, M13, M6, and P3 had greater degree values than the average. AKT1, MAPK1, PIK3CA, and mTOR have degrees of 21, 19, 19, and 13, respectively. These targets were linked to components and KEGG pathways, and they could be useful in the therapy of vitiligo. The PI3K-Akt, TNF, MAPK, and FoxO signaling pathways were also enriched in the KEGG pathway with more than 10 targets. These pathways consistent with previous research[30-32], and they may hold the key to vitiligo treatment. The key nodes and their degree values were listed in Table S6. Furthermore, 13 core targets in PPI were linked to 23 compounds, in which, M30, M10, M13, M6, M15, M24, and P3 had larger degrees. There were 6 targets of the 13 found to be engaged in PI3K-Akt signaling pathway, and 5 in FoxO, mTOR, and MAPK signaling pathways, respectively (as shown in Fig. 5D and Supplement Table S7). The results showed that YQD was a multi-component, multi-target, and multi-pathway treatment for vitiligo.

Molecular docking analysis. Since the accuracy of TCM network pharmacology target prediction is largely dependent on the prediction ability of the network server and the target prediction tool, the prediction data is primarily derived from experiments[33]. However, because the number of drug-target effects verified by experiments was limited, some drugs or compounds with less research had fewer predicted targets. By examining the physical and energetic matching between target protein receptors and drug small molecules to anticipate the interaction between small molecules and targets, high-throughput molecular docking can be utilized as one of the strategies for screening active components and targets. It is widely assumed that the lower the energy of the ligand binding to the receptor, the greater the potential of action. In this study, the active compounds with high, medium, and low degree values in YQD were docked with potential core targets by high-throughput molecular docking, which can make up for the deficiency of network pharmacology studies on the compound with few targets. The results showed that these compounds had a good binding ability with AKT1 (PDB: 4EJN), MAPK1 (PDB: 5K4I), and mTOR (PDB: 5WBH) proteins. Among them, C42 formed hydrogen bonds with amino acids GLN-79, ASP-292, and THR-82 in AKT1 protein, and the docking binding energy was less than -9.0. The CTD network degree values of the compounds and docking parameters with disease targets were shown in Table 6. The top 3 with the best binding affinity between target and active molecules were shown in Fig. 6.

Compounds	Degree	Vina score of compound-target docking (unit: kcal/mol)		
		AKT1	MAPK1	mTOR
M30	24	-9.0	-7.6	-8.4
M24	23	-6.5	-8.6	-8.2
C42	23	-9.5	-7.5	-9.6
M32	13	-7.4	-7.8	-9.5
M10	12	-7.3	-8.8	-11.1
M15	12	-7.2	-9.1	-10.4
M6	9	-10.2	-5.2	-10.1
C31	7	-9.1	-5.5	-11.8
P4	5	-8.7	-5.0	-10.2
C30	4	-8.2	-5.2	-9.0
P2	3	-8.7	-4.7	-8.6

Table 6. Degree and Vina score of compound-target docking.

Effects of YQD on Melanogenesis of Zebrafish. In this study, pericardium edema, yolk absorption delay, and mortality rates of zebrafish within 96 hpf (4 dpf) after YQD treatment were observed to elucidate the acute toxicity of YQD to zebrafish embryos and identify the dose of YQD. The statistical results were shown in Table S8, and the condition of zebrafish larvae in each group 3 dpf after injection was depicted in Supplement Fig. S1A. The results showed that a concentration of YQD below 1000 μg/ml had no influence on zebrafish larvae's pericardium development or yolk absorption, and the larvae's growth and development were normal under the microscope. However, in the 2000 μg/ml group, a considerable number of juvenile fish died, with a mortality rate ranging from 50% to 100%. All embryos died within 3 dpf after the concentration was increased to 4000 μg/ml. The experimental results suggested that when the concentration of YQD solution was 2000 μg/ml or above, it would have a great impact on the development of zebrafish larvae, possibly resulting in a substantial number of deaths. The calculated LC50 was 1997 μg/ml (Supplement Fig. S1B).

Next, we explored whether YQD could increase melanogenesis in vivo. Zebrafish embryos were separated into eight groups and constantly treated with blank culture medium, varying doses of YQD (200~1200 μg/ml), and positive drugs for 84 hpf (3.5 dpf), respectively. The density and distribution of melanin granules were observed and recorded every day. We discovered that as zebrafish embryos grew, the density of melanin in the head and tail increased progressively. The difference between groups peaked at 3.5 dpf, and melanin production in the head, dorsal spine, and abdomen of zebrafish treated with YQD (400~1200 μg/ml) was more noticeable, while the high concentration group did not affect the survival and development of juvenile fish (Fig. 7A).The melanin density in zebrafish tails was measured using Image-Pro Plus image processing software. The results were shown in Fig. 7B, there was a significant difference between the sample group above 400 μg/ml and the blank group.

Discussion

As a common depigmentation skin disorder, vitiligo was led by dysfunction or destruction of melanocytes that were pigment-producing cells[34]. The report demonstrated that antibodies and T lymphocytes can be produced in patients with vitiligo, indicating that the immune response may lead to the destruction of melanocytes[35]. The toxic melanin precursors synthesized by the cells themselves and some chemicals that cause skin depigmentation may also selectively destroy melanocytes. In addition, a large-scale genome-wide association study, primarily targeting whites and Chinese of European descent individuals, identified approximately 56 different genes that contribute to vitiligo risk, and that some genes also contribute to autoimmunity, oxidative stress, and melanogenesis in melanocytes[36]. Therefore, the pathogenesis of vitiligo is complex and there are many associated genes, so it is very urgent to find a specific drug for the treatment of vitiligo.

For many years, YQD has been used in China to treat vitiligo, and it has a remarkable therapeutic effect with few adverse effects. YQD's therapeutic targets and mechanism of action, however, were unknown. Furthermore, the critical elements in YQD were not thoroughly explored, which hampered YQD's in-depth investigation into the treatment of vitiligo. As a result, 44 chemicals in vitro and 36 absorbed components of YQD were identified by UPLC-Q-TOF/MS in this investigation. The major active components and important target genes of YQD in the therapy of vitiligo, as well as the critical signaling route, were then uncovered utilizing network pharmacology. Finally, we investigated how YQD affected zebrafish melanin synthesis.

In this study, a total of 44 chemicals were identified in YQD, including 20 triterpenoids and their glycosides, 10 flavonoids and their glycosides, and other components. There were 16 Astragalus propinquus Schischkin components, 19 Akebiae Fructus components, 13 Leonuri Fructus components, and 2 Caragana Sinica Roots components, with 6 common components. Among them, calceolarioside B (C13), akebia saponin PJ1 (C24), akebia saponin E (C30), akebia saponin D (C31) from Akebiae Fructus and calycosin-7-O-β-D-glucoside (C12) from Astragalus propinquus Schischkin had higher response values, which may be the quality marker of YOD. This study was the first to identify the chemical elements of YQD in vitro, laying the groundwork for the subsequent discovery of absorbed components and prediction of active chemicals.

The results of serum pharmacochemistry in rats after intragastric administration showed that the prototype components of YQD absorbed were from four single herbs and were representative components of each. The metabolites were mainly from the flavonoids in Astragalus propinquus Schischkin, in which one was phase I and 31 were phase II metabolites. Among the phase II metabolites, 3 sulfates, 21 glucuronides, and 4 sulfuric acid and glucuronic acid conjugates were included. Since the components absorbed in the blood are more likely to be bioactive compounds, in this study, 4 prototype components and 22 metabolites of YQD were analyzed by network pharmacology. Simultaneously, components with high in vitro response values and prototype components that produce several metabolites were included in the network pharmacology prediction. According to the results of CTD and CTP network analysis, apigenin (C42), astraisoflavan (M30), apigenin glucuronidation (M10), 7,3',4'-trihydroxyisoflavanone-glucuronidation (M15), formononetin-demethylation (M24), calycosin-7-O-β-D-glucoside (P3) from Astragalus propinquus Schischkin, genkwanin-glucuronidation (M6) from Leonuri Fructus, and akebia saponin D (C31) from Akebiae Fructus may play a crucial role in YQD therapy of vitiligo. Research showed that apigenin may target TRP-1 and TRP-2 through the MAPK pathway, thereby promoting melanin production[37]. Formononetin and astraisoflavan-7-O-β-D-glucoside significantly suppressed concanavalin A (Con A)-induced T lymphocyte proliferation[38], while apigenin, apigenin-7-glucuronic acid, akebia saponin D, and formononetin also had good anti-inflammatory and antioxidant activity[39-42]. Genkwanin had antitumor and immunomodulatory activity [43].

Meanwhile, the important target proteins that participate in the efficacy of YQD were AKT1, TNF, mTOR, PIK3CA, and MAPK1. MITF is the main regulator of gene transcription related to melanin synthesis, which can further upregulate the expression of TYR, TRP-1, and TRP-2, and ultimately stimulate melanin synthesis, while MITF transcription can be increased by inducing AKT1 phosphorylation[30,44,45]. Studies have shown that active compounds induce activation of the mTOR pathway to protect melanocytes from dendritic loss under oxidative stress, thereby maintaining melanin levels in skin pigmentation[46]. The early expression of phosphorylated MAPK1 can upregulate the transcriptional activity of MITF, thereby promoting melanin synthesis[47-49]. GO enrichment analysis showed that vitiligo-related target proteins were involved in a variety of biological functions. In addition, KEGG pathway analysis investigated 20 pathways, the canonical pathways related to vitiligo including cancer-related pathways, endocrine disorders, oxidative stress, inflammation, and antivirals. Among them, PI3K-AKT, FoxO, TNF, and MAPK signaling pathways were enriched in more than 10 targets, suggesting that YQD has a certain intervention effect on these signaling pathways. It was reported that these pathways were involved in the regulation of melanin production[50-55]. The main vitiligo related pathways involved in YQD and the relationship between active components and pathway targets were shown in Fig. 8.

The prediction of component targets in this study was based on network prediction tools, despite the fact that Caragana Sinica Roots in YQD had a long history of medicinal use, there had been few studies on its pharmacological effects and active components, and only three vitiligo-related targets were predicted in this investigation. We chose the substances with the highest, medium, and lowest degree values of active ingredients for docking verification with critical targets in high-throughput molecular docking to prevent missing active chemicals as much as possible. The greatest binding energy of the active compounds with a low degree to the target protein was -4.7 kcal/mol (P2-MAPK1), while the minimum binding energy was -9.0 kcal/mol (C30-mTOR), showing that these active compounds had a good binding capacity to the key targets. We compensated for the flow in network pharmacological prediction by molecular docking of compounds with low degree values. Some TCM components that have received little attention may have a major role in treatment, pointing the way for future research.

For the first time in this work, the in vitro chemical composition spectrum and serum chemical composition spectrum of YQD were determined. Serum pharmacochemistry was used to examine the blood transfer components. The in vitro symbolic components and absorbable components were integrated to predict network pharmacology and verify molecular docking to determine the key active components of YQD in the treatment of vitiligo. The projected results revealed that each herb in the prescription contributed to the active components of YQD, with Astragalus propinquus Schischkin contributing the most. Akebiae Fructus's active ingredients, Leonuri Fructus, and Caragana Sinica Roots, also demonstrated good activity and docking ability. These active components merited further investigation. The results of the investigation revealed that YQD acted as an anti-vitiligo agent via multiple prescriptions, components, and targets.

In addition, we investigated YQD's toxicity in zebrafish and confirmed its influence on melanin formation in animals. The zebrafish genome is highly comparable to the human genome[56], and it has the benefits of tiny size, great reproductive capacity, and a translucent body of juvenile fish, making it a valuable supplement to cell and mammalian models and playing an increasingly important role in drug development[57,58]. Zebrafish is currently a well-renowned biotoxicological model system for high-throughput chemical toxicity testing and is increasingly being used in TCM toxicity research[59]. During growth and development, zebrafish larvae can directly show melanin strips, and zebrafish share genetic similarities with humans in terms of pigment expression via the activation of MITF, TYR, TRP-1, and TRP-2 [60]. As a result, the zebrafish model is commonly employed as a model for in vivo melanin generation[61,62]. Experimental confirmation showed that YQD could speed up the development of new melanin in the heads, backs, and abdomens of zebrafish without affecting their growth and development, implying that YQD might boost melanin production, which is important for treating vitiligo. Other studies demonstrated that MAPK signaling pathway plays an important role in promoting pigmentation in zebrafish[63,64], which was consistent with our predicted results.

There are certain limitations to this study, which employed network pharmacology and a zebrafish model experiment to anticipate the therapeutic components and mechanism of YQD against vitiligo and to verify its efficiency. In this work, the projected active components and related signaling pathways, for example, were not confirmed. We will test these projected components in the future to determine whether the components of YQD are useful in treating vitiligo. We will further test the anti-vitiligo mechanisms of YQD using cell and rat research to examine the relevant pathways.

Conclusions

In conclusion, from the standpoint of serum pharmacochemistry, this work is beneficial to understanding the biological transformation and pharmacological actions of YQD absorption components. Network pharmacology was used to discover the key target proteins and important compounds of YQD in the

treatment of vitiligo, including apigenin, astraisoflavan, akebia saponin D, genkwanin glucuronidation metabolites and apigenin-glucuronidation metabolites, AKT1, MAPK1, and mTOR, based on the in vitro symbolic components and the absorption compounds of YQD that were analyzed by UPLC-Q-TOF/MS. The major signaling mechanism of YQD against vitiligo was also investigated using KEGG enrichment analysis, which included the PI3K-AKT, FoxO, mTOR, and MAPK signaling pathways. The active molecules displayed a good binding ability to important targets, according to the molecular docking results. Furthermore, experimental confirmation found that YQD might boost zebrafish melanin synthesis, which could verify its role in the treatment of vitiligo.

Abbreviations

YQD:	Yiqi Qubai Decoction
UPLC-Q-TOF/MS:	Ultrahigh performance liquid chromatography coupled with quadrupole-time of flight mass spectrometry
TCM:	Traditional Chinese medicine
CTD:	Compound-target-disease
PPI:	Protein-protein interaction
CTP:	Component-target-pathway
KEGG:	Kyoto Encyclopedia of Genes and Genomes
GO:	Gene Ontology
mTOR:	Mammalian target of rapamycin
MAPK1:	Mitogen-activated Protein Kinase 1
PI3K:	Phosphoinositide 3-kinase
AKT:	Serine-threonine kinase
FoxO:	Forkhead box, class O
TNF:	Tumor Necrosis Factor
MITF:	Microphthalmia-associated transcription factor
TYR:	Tyrosinase
TRP-1:	Tyrosinase-related proteins 1
TRP-2:	Tyrosinase-related protein 2

Declarations

Data Availability

The data used to support the findings of this study are include in the article.

Ethics Statement

Ethics Approval: Rat, was maintained, handled, and bred according to standard protocols from the Institutional Animal Care and Use Committee of Shanghai Jiao Tong University (IACUC A2018075). Adult and larvae zebrafish were maintained, handled, and bred according to standard protocols from the Institutional Animal Care and Use Committee of Shanghai Jiao Tong University (IACUC 202101310). Animal studies were carried out in accordance with the Guiding Principles for Care and Use of Laboratory Animals and followed the guidelines for the ethical review of laboratory animal welfare People's Republic of China National Standard GB/T 35892-2018.

Author Contributions

Guorong Fan: Funding acquisition, Project administration, Supervision, Conceptualization, Writing - Review & Editing; **Yuefen Lou:** Project administration, Supervision; **Zhenghua Wu:** Project administration, Supervision; **Lijun Cui:** Conceptualization, Software, Investigation, Resources, Writing-Original Draft; **Cui Ma:** Investigation, Resources; **Wenqing Shi:** Investigation; **Chen Yang:** Writing-Review & Editing; **Jiangping Wu:** Investigation, Resources.

Funding

This work is supported by the National Natural Science Foundation of China (81793289); National Key Clinical Specialty Discipline Construction Program of China (02. DY11.03.19.03); Special fund for clinical research of Wu Jieping Medical Foundation (320.6750.2021-2-75).

Disclosure

The authors declare that they have no conflicts of interest.

Supplementary Materials

The data used to support the findings of this study are available in Supplementary Tables S1 S8 and Figure S1. (*Supplementary Materials*)

References

1. Krüger, C. & Schallreuter, K. U. A review of the worldwide prevalence of vitiligo in children/adolescents and adults. *Int J Dermatol* **51**, 1206–1212 (2012).
2. Bergqvist, C. & Ezzedine, K. Vitiligo: A Review. *Dermatology* **236**, 571–592 (2020).
3. Razmi T, M., Afra, T. P. & Parsad, D. Vitiligo surgery: A journey from tissues via cells to the stems. *Exp Dermatol* **28**, 690–694 (2019).
4. Zubair, R. & Hamzavi, I. H. Phototherapy for Vitiligo. *Dermatol Clin* **38**, 55–62 (2020).
5. Jung, H. M., Jung, Y. S., Lee, J. H., Kim, G. M. & Bae, J. M. Antioxidant supplements in combination with phototherapy for vitiligo: A systematic review and metaanalysis of randomized controlled trials. *J Am Acad Dermatol* **85**, 506–508 (2021).
6. Seneschal, J. *et al.* Efficacy and Safety of Tacrolimus 0.1% for the Treatment of Facial Vitiligo: A Multicenter Randomized, Double-Blinded, Vehicle-Controlled Study. *J Invest Dermatol* **141**, 1728–1734 (2021).
7. Wada-Irimada, M. *et al.* Efficacy and safety of i.v. methylprednisolone pulse therapy for vitiligo: A retrospective study of 58 therapy experiences for 33 vitiligo patients. *J Dermatol* **48**, 1090–1093 (2021).
8. Yang, K. Y. The effect of 308nm excimer light combined with Yiqiqubai granule on the treatment of vitiligo ,2016.
9. Zhang, C., Zhou, L., Huang, J. & Shi, W. A combination of Yiqiqubai granule and 308-nm excimer laser in treatment of segmental vitiligo: a prospective study of 233 patients. *J Dermatolog Treat* **28**, 668–671 (2017).
10. Fu, J. *et al.* Review of the botanical characteristics, phytochemistry, and pharmacology of Astragalus membranaceus (Huangqi). *Phytother Res* **28**, 1275–1283 (2014).
11. Gong, A., Duan, R., Wang, H. Y., Kong, X. P., Dong, T., Tsim, K. & Chan, K. Evaluation of the Pharmaceutical Properties and Value of Astragali Radix. *Medicines (Basel)* **5**, (2018).
12. Jiang, H., Gu, S. L., Zhang, Y. T. & Fan, C. Advances in Chemical Constituents and Pharmacological Effects of Astragalus membranaceus. *J Anhui Univ Chinese Med* **39**, 93–96 (2020).
13. Ma, B. *et al.* An integrated study of metabolomics and transcriptomics to reveal the anti-primary dysmenorrhea mechanism of Akebiae Fructus. *J Ethnopharmacol* **270**, 113763 (2021).
14. Wang, H. *et al.* Structural properties and in vitro and in vivo immunomodulatory activity of an arabinofuranan from the fruits of Akebia quinata. *Carbohydr Polym* **256**, 117521 (2021).
15. Zhang, N., Wang, M., Li, Y., Zhou, M., Wu, T. & Cheng, Z. TLC-MS identification of alkaloids in Leonuri Herba and Leonuri Fructus aided by a newly developed universal derivatisation reagent optimised by the response surface method. *Phytochem Anal* **32**, 242–251 (2021).
16. Shu P.H., L. *et al.* Research progress on chemical constituents and pharmacological activities of Frutus Leonuri. *Chinese Archives of Traditional Chinese Medicine* 1–12 (2022).
17. Meng, Q., Niu, Y., Niu, X., Roubin, R. H. & Hanrahan, J. R. Ethnobotany, phytochemistry and pharmacology of the genus Caragana used in traditional Chinese medicine. *J Ethnopharmacol* **124**, 350–368 (2009).
18. Jin, Q. *et al.* Antioxidative oligostilbenes from Caragana sinica. *Bioorg Med Chem Lett* **22**, 973–976 (2012).
19. Wu, Y., Liu, X. & Li, G. Integrated bioinformatics and network pharmacology to identify the therapeutic target and molecular mechanisms of Huangqin decoction on ulcerative Colitis. *Sci Rep* **12**, 159 (2022).
20. Lu, X. *et al.* Study of the active ingredients and mechanism of Sparganii rhizoma in gastric cancer based on HPLC-Q-TOF-MS/MS and network pharmacology. *Sci Rep* **11**, 1905 (2021).
21. Saikia, S. & Bordoloi, M. Molecular Docking: Challenges, Advances and its Use in Drug Discovery Perspective. *Curr Drug Targets* **20**, 501–521 (2019).
22. Zhang, M., Yang, J., Zhao, X., Zhao, Y. & Zhu, S. Network pharmacology and molecular docking study on the active ingredients of qidengmingmu capsule for the treatment of diabetic retinopathy. *Sci Rep* **11**, 7382 (2021).
23. Wu, Z. *et al.* Schisandrol A, the main active ingredient of Schisandrae Chinensis Fructus, inhibits pulmonary fibrosis through suppression of the TGF-β signaling pathway as revealed by UPLC-Q-TOF/MS, network pharmacology and experimental verification. *J Ethnopharmacol* **289**, 115031 (2022).
24. **Commission, C. P.** *Pharmacopoeia of the People's Republic of China*. Beijing: China Medical Science Press, 2020, p.252,315.
25. Ma, D. Y. & Hu, C. Q. Studies on chemical constituents from roots of Caragana sinica. *Zhongguo Zhong Yao Za Zhi* **33**, 517–521 (2008).
26. Xue, Z. & Yang, B. Phenylethanoid Glycosides: Research Advances in Their Phytochemistry, Pharmacological Activity and Pharmacokinetics. *Molecules* **21**, (2016).
27. Chen, W. *et al.* Validated UHPLC-MS/MS method for simultaneous determination of four triterpene saponins from Akebia trifoliata extract in rat plasma and its application to a pharmacokinetic study. *Biomed Chromatogr* **33**, e4585 (2019).
28. Li, P. *et al.* Pharmacokinetics, Bioavailability, Excretion and Metabolism Studies of Akebia Saponin D in Rats: Causes of the Ultra-Low Oral Bioavailability and Metabolic Pathway. *Front Pharmacol* **12**, 621003 (2021).
29. Chen, J. X., Chen, R. Y., Lian, Y., Yao, X. S., Huang, Y. X., Gao, Y. X. & Y. Progress in Microbial Conversion and Functional Activity of Soy Isoflavones. *Shipin Yanjiu Yu Kaifa* **42**, 176–182 (2021).
30. Niu, C., Yin, L. & Aisa, H. A. Novel Furocoumarin Derivatives Stimulate Melanogenesis in B16 Melanoma Cells by Up-Regulation of MITF and TYR Family via Akt/GSK3β/β-Catenin Signaling Pathways. *Int J Mol Sci* **19**, (2018).

31. Lei, Z. *et al.* Identification of key genes and pathways involved in vitiligo development based on integrated analysis. *Medicine (Baltimore)* **99**, e21297 (2020).
32. Singh, M., Mansuri, M. S., Kadam, A., Palit, S. P., Dwivedi, M., Laddha, N. C. & Begum, R. Tumor Necrosis Factor-alpha affects melanocyte survival and melanin synthesis via multiple pathways in vitiligo. *Cytokine* **140**, 155432 (2021).
33. Meng, F. C. & Tang, L. D. Challenges and prospect in research of Chinese materia medica network pharmacology. *Chinese Traditional and Herbal Drugs* **51**, 2232–2237 (2020).
34. Shumway, D. A., Abu-Isa, E., Soto, D. E., Do, T. T. & Jagsi, R. Depigmentation Within the Radiation Field in Patients With Vitiligo. *Int J Radiat Oncol Biol Phys* **94**, 421–422 (2016).
35. Moftah, N. H., El-Barbary, R. A., Ismail, M. A. & Ali, N. A. Effect of narrow band-ultraviolet B on CD4(+) CD25(high) FoxP3(+) T-lymphocytes in the peripheral blood of vitiligo patients. *Photodermatol Photoimmunol Photomed* **30**, 254–261 (2014).
36. Wang, J. Y. *et al.* Network pharmacological mechanisms of Vernonia anthelmintica (L.) in the treatment of vitiligo: Isorhamnetin induction of melanogenesis via up-regulation of melanin-biosynthetic genes. *BMC Syst Biol* **11**, 103 (2017).
37. Liu-Smith, F. & Meyskens, F. L. Molecular mechanisms of flavonoids in melanin synthesis and the potential for the prevention and treatment of melanoma. *Mol Nutr Food Res* **60**, 1264–1274 (2016).
38. Zhang, W. W., Xu, F., Wang, D., Ye, J. & Cai, S. Q. Buyang Huanwu Decoction ameliorates ischemic stroke by modulating multiple targets with multiple components: In vitro evidences. *Chin J Nat Med* **16**, 194–202 (2018).
39. Gu, M. *et al.* Akebia Saponin D suppresses inflammation in chondrocytes via the NRF2/HO-1/NF-κB axis and ameliorates osteoarthritis in mice. *Food Funct* **11**, 10852–10863 (2020).
40. Wang, X., Ding, G., Liu, B. & Wang, Q. Flavonoids and antioxidant activity of rare and endangered fern: Isoetes sinensis. *PLoS One* **15**, e0232185 (2020).
41. Huang, J., Chen, X. & Xie, A. Formononetin ameliorates IL-13-induced inflammation and mucus formation in human nasal epithelial cells by activating the SIRT1/Nrf2 signaling pathway. *Mol Med Rep* **24**, (2021).
42. Sugimoto, M., Ko, R., Goshima, H., Koike, A., Shibano, M. & Fujimori, K. Formononetin attenuates H(2)O(2)-induced cell death through decreasing ROS level by PI3K/Akt-Nrf2-activated antioxidant gene expression and suppressing MAPK-regulated apoptosis in neuronal SH-SY5Y cells. *Neurotoxicology* **85**, 186–200 (2021).
43. Wang, X. *et al.* Antitumor and immunomodulatory activity of genkwanin on colorectal cancer in the APC(Min/+) mice. *Int Immunopharmacol* **29**, 701–707 (2015).
44. Zang, D., Niu, C. & Aisa, H. A. Amine derivatives of furocoumarin induce melanogenesis by activating Akt/GSK-3β/β-catenin signal pathway. *Drug Des Devel Ther* **13**, 623–632 (2019).
45. Liu, B., Xie, Y. & Wu, Z. Astragaloside IV Enhances Melanogenesis via the AhR-Dependent AKT/GSK-3β/β-Catenin Pathway in Normal Human Epidermal Melanocytes. *Evid Based Complement Alternat Med* **2020**, 8838656 (2020).
46. Wan, J., Lin, F., Zhang, W., Xu, A., DeGiorgis, J., Lu, H. & Wan, Y. Novel approaches to vitiligo treatment via modulation of mTOR and NF-κB pathways in human skin melanocytes. *Int J Biol Sci* **13**, 391–400 (2017).
47. Jung, E. *et al.* Afzelin positively regulates melanogenesis through the p38 MAPK pathway. *Chem Biol Interact* **254**, 167–172 (2016).
48. Li, P. H., Liu, L. H., Chang, C. C., Gao, R., Leung, C. H., Ma, D. L. & David Wang, H. M. Silencing Stem Cell Factor Gene in Fibroblasts to Regulate Paracrine Factor Productions and Enhance c-Kit Expression in Melanocytes on Melanogenesis. *Int J Mol Sci* **19**, (2018).
49. Shin, S., Ko, J., Kim, M., Song, N. & Park, K. Morin Induces Melanogenesis via Activation of MAPK Signaling Pathways in B16F10 Mouse Melanoma Cells. *Molecules* **26**, (2021).
50. Hah, Y. S. *et al.* Induction of melanogenesis by rapamycin in human MNT-1 melanoma cells. *Ann Dermatol* **24**, 151–157 (2012).
51. Kim, J., Choi, H., Cho, E. G. & Lee, T. R. FoxO3a is an antimelanogenic factor that mediates antioxidant-induced depigmentation. *J Invest Dermatol* **134**, 1378–1388 (2014).
52. Tsao, Y. T. *et al.* Hinokitiol Inhibits Melanogenesis via AKT/mTOR Signaling in B16F10 Mouse Melanoma Cells. *Int J Mol Sci* **17**, 248 (2016).
53. Zhou, S. & Sakamoto, K. Pyruvic acid/ethyl pyruvate inhibits melanogenesis in B16F10 melanoma cells through PI3K/AKT, GSK3β, and ROS-ERK signaling pathways. *Genes Cells* **24**, 60–69 (2019).
54. Moon, K. M., Lee, M. K., Hwang, T., Choi, C. W., Kim, M. S., Kim, H. R. & Lee, B. The multi-functional roles of forkhead box protein O in skin aging and diseases. *Redox Biol* **46**, 102101 (2021).
55. Mosca, S., Cardinali, G., Flori, E., Briganti, S., Bottillo, I., Mileo, A. M. & Maresca, V. The PI3K pathway induced by αMSH exerts a negative feedback on melanogenesis and contributes to the release of pigment. *Pigment Cell Melanoma Res* **34**, 72–88 (2021).
56. Barbazuk, W. B. *et al.* The syntenic relationship of the zebrafish and human genomes. *Genome Res* **10**, 1351–1358 (2000).
57. Zhong, Z., Li, Y., Chen, Y., Chen, W., Li, S., Lv, X. & Luo, S. Predicting and Exploring the Mechanisms of Erzhi Pill in Prevention and Treatment of Osteoporosis Based on Network Pharmacology and Zebrafish Experiments. *Drug Des Devel Ther* **15**, 817–827 (2021).
58. Cai, Z. *et al.* Elaborate the Mechanism of Ancient Classic Prescriptions (Erzhi Formula) in Reversing GIOP by Network Pharmacology Coupled with Zebrafish Verification. *Evid Based Complement Alternat Med* **2022**, 7019792 (2022).
59. Jayasinghe, C. D. & Jayawardena, U. A. Toxicity Assessment of Herbal Medicine Using Zebrafish Embryos: A Systematic Review. *Evid Based Complement Alternat Med* **2019**, 7272808 (2019).
60. Singh, A. P. & Nüsslein-Volhard, C. Zebrafish stripes as a model for vertebrate colour pattern formation. *Curr Biol* **25**, R81-R92 (2015).

61. Lv, J., An, X., Jiang, S., Yang, Y., Song, G. & Gao, R. Protoporphyrin IX Stimulates Melanogenesis, Melanocyte Dendricity, and Melanosome Transport Through the cGMP/PKG Pathway. *Front Pharmacol* **11**, 569368 (2020).
62. Abbas, Q., Ashraf, Z., Hassan, M., Nadeem, H., Latif, M., Afzal, S. & Seo, S. Y. Development of highly potent melanogenesis inhibitor by in vitro, in vivo and computational studies. *Drug Des Devel Ther* **11**, 2029–2046 (2017).
63. Kim, Y. M., Lim, H. M., Ro, H. S., Ki, G. E. & Seo, Y. K. Pulsed Electromagnetic Fields Increase Pigmentation through the p-ERK/p-p38 Pathway in Zebrafish (Danio rerio). *Int J Mol Sci* **19**, (2018).
64. Kim, Y. M., Lee, E. C., Lim, H. M. & Seo, Y. K. Rice Bran Ash Mineral Extract Increases Pigmentation through the p-ERK Pathway in Zebrafish (Danio rerio). *Int J Mol Sci* **20**, (2019).

Figures

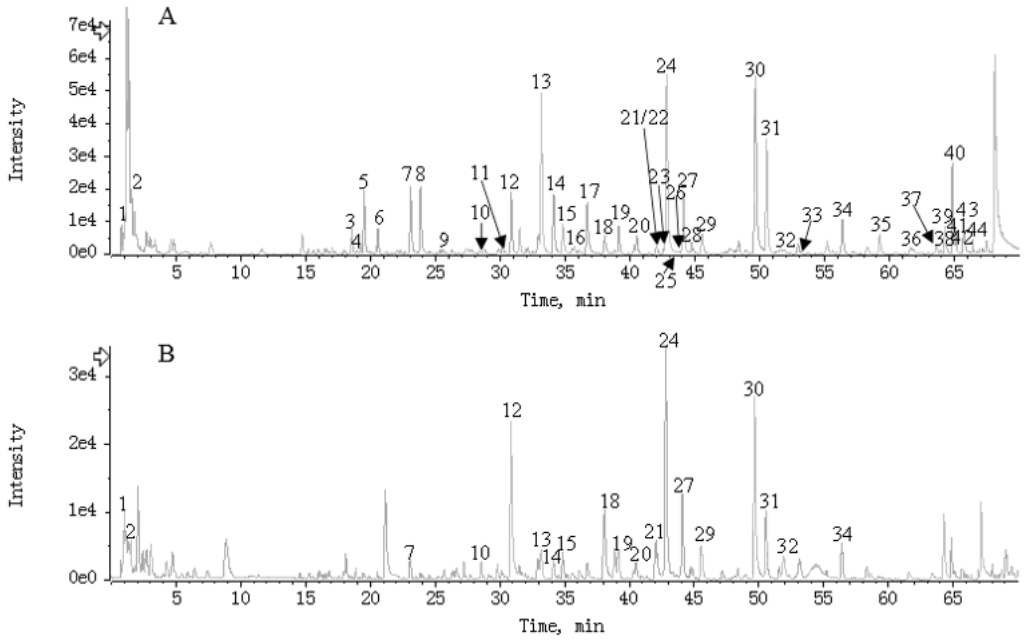


Figure 1

(A) UPLC-HRMS Base Peak Chromatogram (BPC) of YQD sample- negative ion mode. (B) UPLC-HRMS Base Peak Chromatogram (BPC) of YQD sample- positive ion mode.

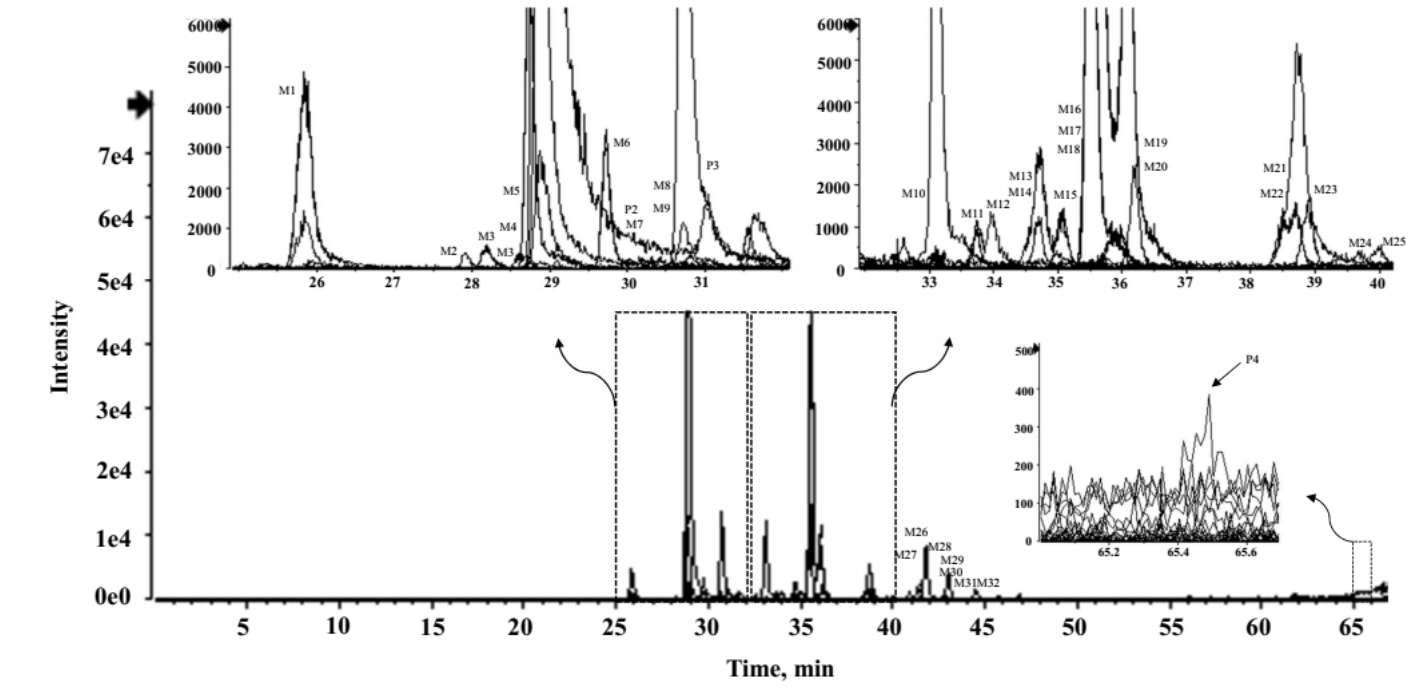


Figure 2

Extracted ion chromatograms (EIC) of absorbed components and metabolites after intragastric administration of YQD at 1 h.

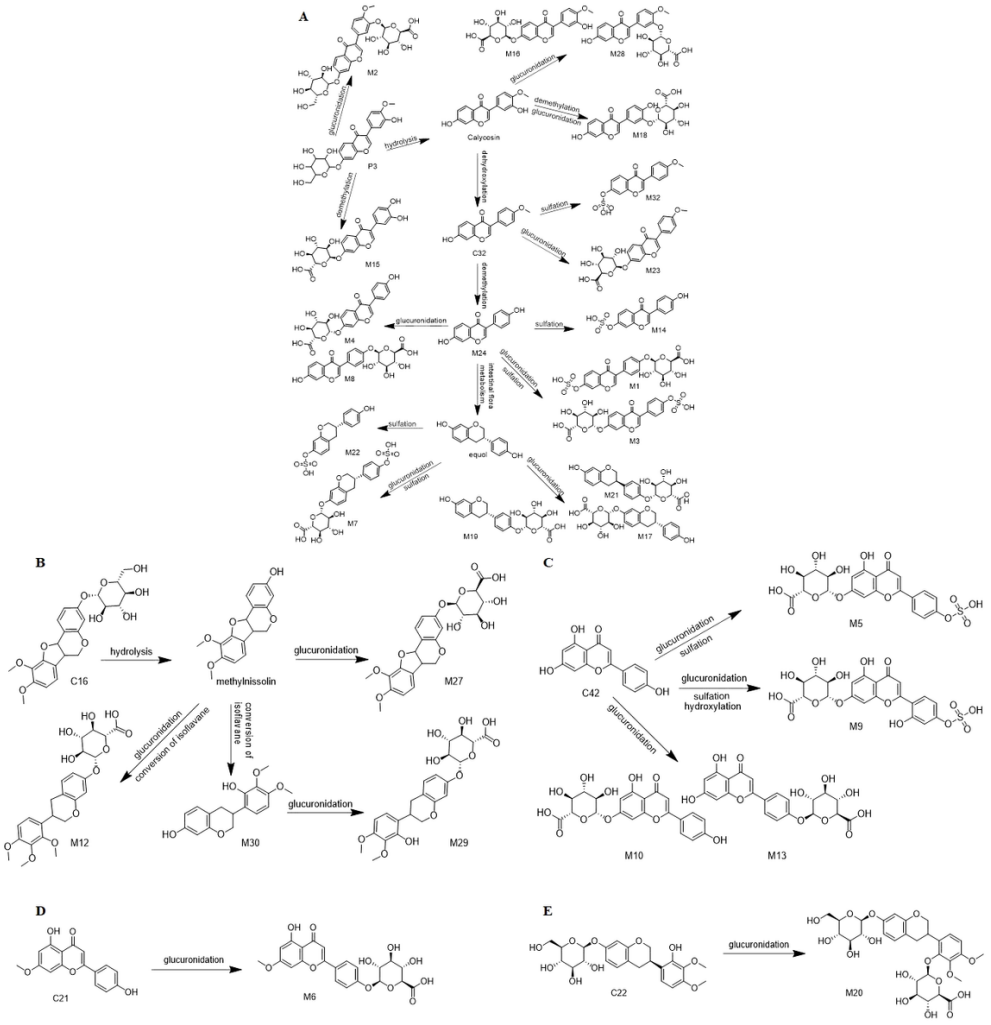


Figure 3

Possible metabolic pathways of 32 metabolites in rats after intragastric administration of YQD. (A) Calycosin-7-O-β-D-glucoside. (B) Methylnissolin-3-O-glucoside. (C) Apigenin. (D) Astraisoflavan-7-O-β-D-glucoside. (E) Genkwanin.

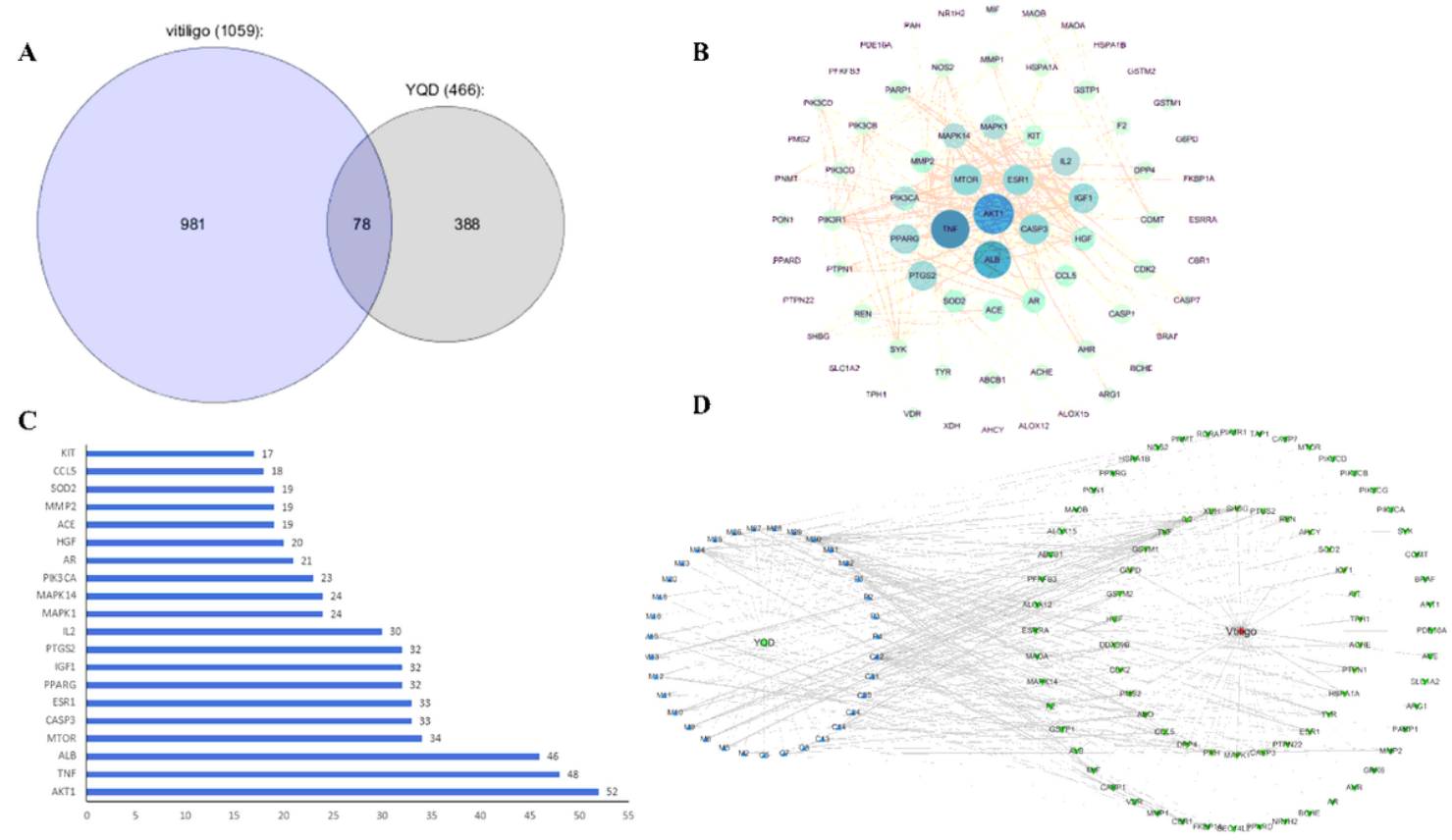


Figure 4

(A) Venn diagram of related targets of YQD and Vitiligo. (B)In visualization analysis of the PPI diagram, the size of the circle represents the target degree. (C) Several adjacent nodes of overlapping targets between YQD and vitiligo, the X-axis represents the number of adjacent proteins of the target and the Y-axis represents different targets. (D) Component-target-disease network (31 components(blue) were connected to 78 target genes(green) and YQD (red), 78 target genes(green) were connected to 31 components(blue) and vitiligo (yellow)).

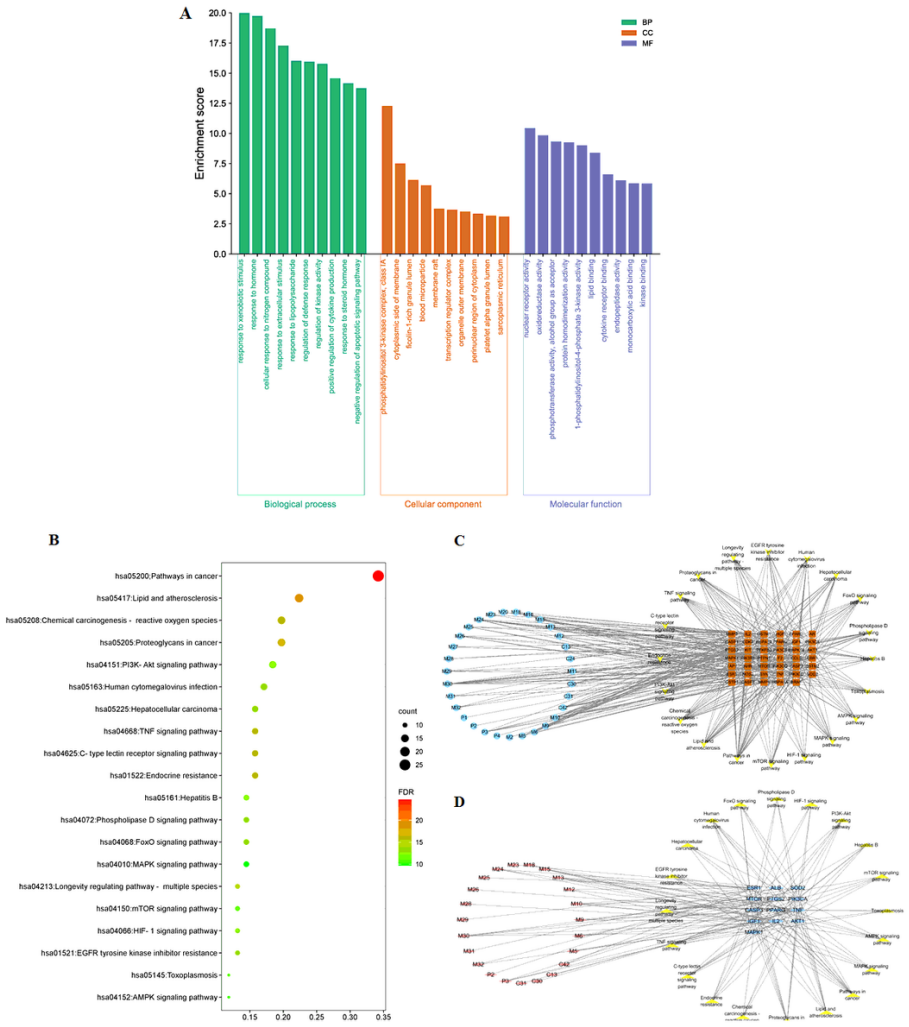


Figure 5

(A) GO analysis. (B) Top 20 enriched KEGG pathways. (C) Component-target-pathway network (Components (blue) were connected to 41 target genes. Target genes (orange) were connected to 20 pathways (yellow) and 31components). (D) Core targets- component -pathway network (13 core targets were connected to 20 pathways (yellow) and 23 components.

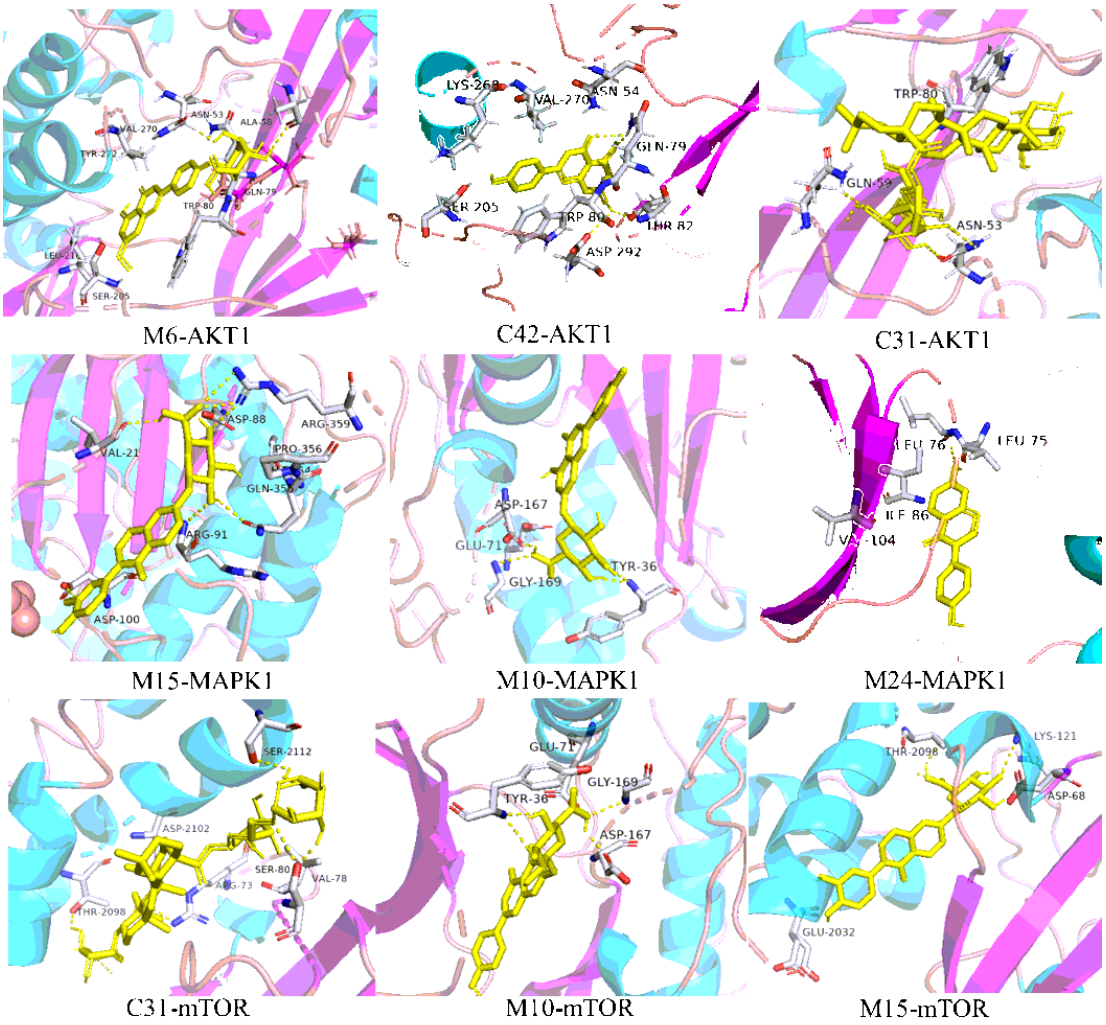


Figure 6

Molecular docking of compounds with target proteins

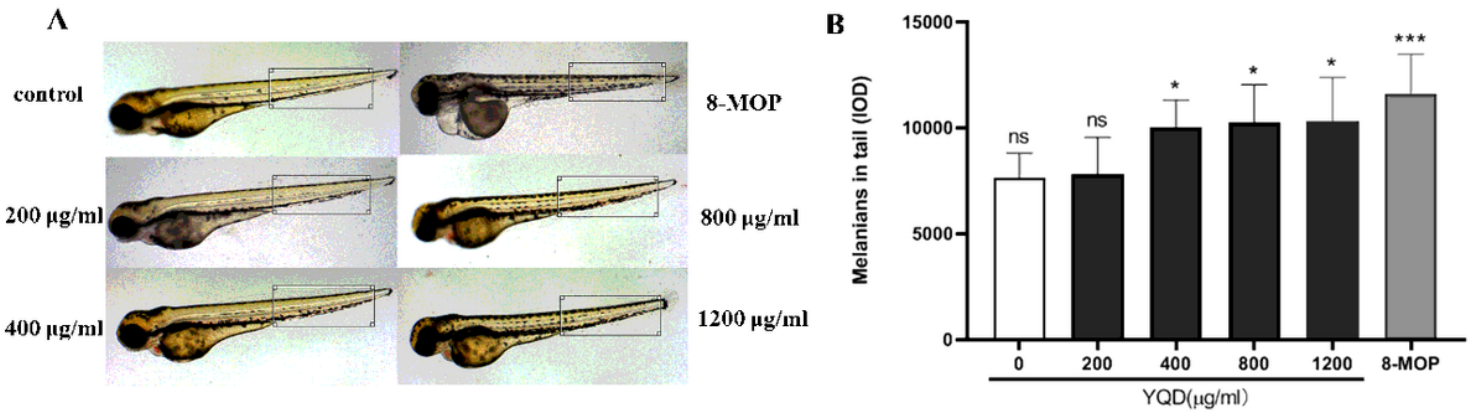


Figure 7

(A) Growth status of zebrafish after 3.5 dpf administration. (B) Effect of YQD on melanin formation in zebrafish.

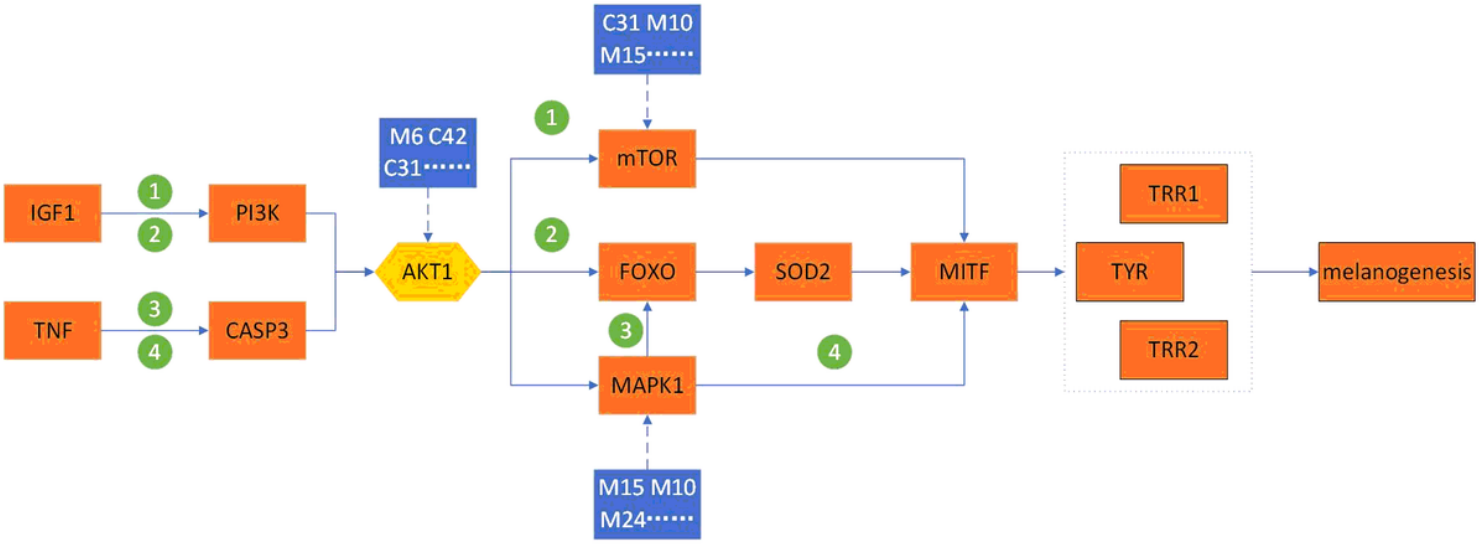


Figure 8

The main pathways and targets involved in YQD related to vitiligo and their relationship with active compounds.

Supplementary Files

This is a list of supplementary files associated with this preprint. Click to download.

- FigureS1.pdf
- TableS1.pdf
- TableS2.pdf
- TableS3.pdf
- TableS4.pdf
- TableS5.pdf
- TableS6.pdf
- TableS7.pdf
- TableS8.pdf